RSC Advances

PAPER

View Article Online
View Journal | View Issue

Cite this: *RSC Adv.*, 2026, **16**, 6507

Exploring coconut shell-derived activated carbon black as a green alternative for toner colourants

G. D. M. H. Wijewardhana,[a] T. B. N. S. Madugalla,[b] M. M. M. G. P. G. Mantilaka,[*a] W. P. S. L. Wijesinghe[c] and W. S. S. Gunathilake[d]

Coconut shells (CS) are a promising renewable precursor for carbon black synthesis. By optimising carbonisation parameters for CB synthesis and introducing a low-temperature alkali treatment method using KOH, this study investigates the potential of utilising CS-derived activated carbon black (ACB) as a sustainable black colourant in electrically conductive toner powders. The most efficient synthesis parameters were determined by analysing 36 CB samples that were produced by combining three variables: carbonisation temperature, carbonisation duration, and particle size. The best CB sample was treated using different weight ratios of KOH at 120 °C. The results obtained from FT-IR, XRD, and SEM coupled with EDS, EIS, and TGA revealed that optimised carbonisation and low-temperature KOH treatment caused well-defined porous structures with an amorphous nature. Increasing KOH concentrations result in the formation of large spherical micropores (0.656 μm), however, excessive concentrations lead to smaller or closed pores. The ACB sample synthesised with lower KOH concentration showed the lowest resistance, thermal stability up to 400 °C, and low moisture and ash content. The reduced resistance indicates enhanced electrical conductivity, suggesting the potential of synthesised ACB as a conducting agent, while its high thermal stability indicates suitability for high-temperature printing applications. Moreover, high carbon content (69.2 wt%) and fine particle size (10–15 μm) may ensure good dispersion in polymer matrices while facilitating uniform colour and print quality. Hence the synthesised ACB samples with the lowest KOH concentrations could be used as a black colourant and a conducting agent in the synthesis of toner powders.

Received 13th November 2025
Accepted 27th December 2025

DOI: 10.1039/d5ra08767h

rsc.li/rsc-advances

1 Introduction

Carbon black (CB) is the most common pigment used in black colour printing toner powders because of its higher tinting strength compared to iron black or organic pigments.[1,2] However, commercially available CB is still considered an expensive material, due to the use of nonrenewable and relatively expensive starting materials such as coal and lignite.[3–5] Therefore, in recent years, growing research interest in the production of CB from renewable and cheaper precursors, which are mainly from agricultural byproducts such as coconut shells (CSs), bamboo, wood, rice husk, wheat straw, and coffee bean skin has been encouraged.[6–8] Among these natural resources, CSs are the best material for the synthesis of CB because of their excellent natural structure with a hard and strong texture, which is due to high lignin and carbon content.[9–11] Similarly, higher water solubility, higher reactivity, and low ash content contribute to their hardness and strength properties.[9,12]

Coconut (*Cocos nucifera*) is an abundantly grown plant in most regions of Sri Lanka and the local coconut industry generates a relatively large amount of CS and husk biomass which is thrown away as waste or burned away causing various environmental problems.[13,14] Conversion of CS waste into CB adds economic value to the agro waste, reduces the cost of waste disposal, and provides a potentially inexpensive alternative to the commercially available CB.[15,16] Moreover, the low cost, higher availability, and renewability of CSs make them an ideal source of raw material for the production of CB for various industrial applications.[17–19] To date, different methodologies have been proposed to synthesise CB from CSs such as pyrolysis, gasification, and self-sustained carbonisation.[20–22] Additionally, various properties inherent to the CBs are a result of their carbonisation process.[23] Physical activation, chemical activation, and metal impregnation can further enhance the surface characteristics of CS-derived CB by creating porosity, thereby leading to the formation of activated carbon black (ACB).[24–26] Furthermore, ACBs with diverse pore size

[a]*Postgraduate Institute of Science, University of Peradeniya, Peradeniya, Sri Lanka. E-mail: mantilaka.publications@gmail.com*

[b]*Department of Physical Sciences, Faculty of Applied Sciences, South Eastern University of Sri Lanka, Sammanthurai, Sri Lanka*

[c]*Sri Lanka Institute of Nanotechnology, Nanotechnology & Science Park, Mahewatta, Pitipana, Homagama, Sri Lanka*

[d]*Department of Chemistry, Faculty of Science, University of Peradeniya, Peradeniya, Sri Lanka*

distributions and structures can be produced by varying the activation method, activating agent, and activation conditions.[14,23,27]

Despite the numerous attempts to synthesise ACB from CSs for various applications such as water purification, adsorption processes, and energy storage, there has been less emphasis on its application specifically in electrophotographic toners.[18,28] Currently, toner powders are synthesised using synthetic magnetite and CB.[29] Hence, the utilisation of ACB derived from CS waste as the black colourant in toner powders will increase the demand for CS thereby reducing unwanted, low-value agricultural byproducts and underutilised crops into useful high-value materials.[5] Additionally, higher stability, mechanical strength, higher electrical and thermal conductivity, and low ash content of CS-based ACB will facilitate the best quality printing.[30]

Although CS-derived ACB has found utility across various chemical and industrial sectors, its application in electrically conductive toner formulations has not yet been documented. Existing studies on CS-derived carbons predominantly target enhancements in porosity and specific surface area to optimise performance in adsorption and energy-storage systems. Such characteristics, however, are inherently unsuitable for electrophotographic toner technologies, which demand controlled electrical conductivity, appropriate bulk density, and favourable particle–particle interactions to ensure efficient charge transport and homogeneous incorporation with auxiliary toner components. Addressing this critical gap, the present work establishes a novel route for producing a fully bio-derived, sustainable, and economically advantageous black colourant, thereby transforming abundantly available Sri Lankan CS waste into a high-value functional material. In this context, this study aimed to explore the feasibility of utilising CS-derived ACB as a sustainable black colourant for the formulation of electrically conductive toner powders. Moreover, optimised carbonisation parameters and a low-temperature alkali treatment using KOH were introduced to synthesise ACB from CS waste. The effects of carbonisation parameters and activation conditions on the characteristics of CS-derived ACBs were evaluated.

2 Experimental

2.1 Raw materials

The CSs were collected from a local seller in Kandy district, Sri Lanka. Analytical grade potassium hydroxide (KOH) with a purity of 90.6% was used as the activating agent. Deionised water (DIW) was used throughout the experiments to minimise the contaminations.

2.2 Synthesis of CB utilising CS waste

The CSs were initially cleaned to remove husk and soil particles. They were then soaked in a water bath for 24 hours to facilitate the further removal of impurities attached to the surface of the shells. After soaking, CSs were thoroughly washed with distilled water and dried at 105 °C for 24 h in an oven.[31,32] Once dried, the CSs were crushed with a cleaned hammer, then ground using the disc mill, and sieved to obtain the desired particle sizes. Each crucible was loaded with 10 g of ground CSs, which were then carbonised in the muffle furnace (HOBE.HD-230 PAD; maximum temperature 1200 °C) available at the Department of Geology, University of Peradeniya, Peradeniya, Sri Lanka. A series of experiments were conducted to study the effects of different carbonisation parameters such as particle size of CSs (0.1 mm, 1.0 mm, 2.0 mm, and 5.0 mm), carbonisation temperature (450 °C, 500 °C and 550 °C), and duration of carbonisation (2 h, 3 h, and 4 h) on the characteristics of the CS-based CB. The preparation conditions and sample identification codes of the CBs are listed in Table 1. Following the carbonisation process, each CB sample was allowed to cool to room temperature, washed with distilled water to remove the ash content from the surface, and dried at 105 °C for 24 h in an oven. Then these CB samples were crushed using mortar and pestle and sieved using a mechanical shaker to obtain predetermined size fractions.

2.3 Activation of CB using KOH

The best CB sample, C4a, which was made from 0.1 mm CS particles carbonised at 550 °C for 4 hours, was chosen for activation out of the 36 CB samples made using different combinations of carbonisation parameters based on the results of the FT-IR and SEM. The selected CB sample was crushed and sieved under 43 μm mesh size and 2 g of powdered CB was subjected to an alkali treatment using KOH. Here to identify the effect of weight ratio, 2 g of CB was treated with 4 g, 8 g, and 12 g of KOH (the CB to KOH ratio 1 : 2, 1 : 4, 1 : 6 [w/w]) separately and the samples were labelled as C4a-1, C4a-2, and C4a-3 respectively. 40 ml of DI was used to disperse the mixture, and the samples were stirred continuously at 120 °C using a magnetic stirrer with a hot plate until complete evaporation of all liquid quantity. Next, the ACB samples were washed with 1 M HCl solution, followed by deionised water to remove any KOH residue from the material until the samples achieved pH 7–8. At last, neutralised samples were dried under 105 °C for 24 hours.

2.4 Characterisation of CS, carbonised products and ACBs

The raw CS particles, carbonised samples, and optimally prepared ACB products were characterised by using different analytical techniques. The surface functional groups of samples were analysed using the Fourier-transformed infrared (FT-IR) spectrometer (PerkinElmer FT-IR C95033) equipped with MIRacle ATR (Attenuated Total Reflectance) and a ZnSe crystal available at Science Research Center, Faculty of Applied Science, South Eastern University of Sri Lanka, Sammanthurai, Sri Lanka. The surface morphology was observed using a Scanning Electron Microscope (SEM) analyser (ZEISS EVO LS15) available at the Department of Geology, University of Peradeniya, Peradeniya, Sri Lanka. The samples were studied under magnification from 5.00k× to 10.00k×. The crystalline structure of the samples was analysed using an X-ray powder diffractometer (PANanalytical Emperian) available at Surface and Material Science core labs, KUAST, Abu Dhabi, UAE for the range 5–90°

Table 1 Experimental design matrix for the synthesis of CB from CS waste

Sample nos	Sample codes	Calcination temperature/°C	Duration of calcination/h	Particle size/mm
1–4	A2a–A2d	450	2	0.1, 1.0, 2.0, 5.0
5–8	A3a–A3d	450	3	0.1, 1.0, 2.0, 5.0
9–12	A4a–A4d	450	4	0.1, 1.0, 2.0, 5.0
13–16	B2a–B2d	500	2	0.1, 1.0, 2.0, 5.0
17–20	B3a–B3d	500	3	0.1, 1.0, 2.0, 5.0
21–24	B4a–B4d	500	4	0.1, 1.0, 2.0, 5.0
25–28	C2a–C2d	550	2	0.1, 1.0, 2.0, 5.0
29–32	C3a–C3d	550	3	0.1, 1.0, 2.0, 5.0
33–36	C4a–C4d	550	4	0.1, 1.0, 2.0, 5.0

(2θ) operated at 45 kV, 40 mA with a scan speed of 0.21° s^{-1}, step size of 0.026°, and time per step 30 s.

The electrochemical behaviour of the carbonised CB and ACBs was studied by Electrochemical Impedance Spectroscopic (EIS) analysis using a Metrohm PGSTAT204 electrochemical workstation (Serial No: AUT50184) available at the Department of Chemistry, University of Peradeniya, Peradeniya, Sri Lanka, following the methodology reported in a previous study.[33] Electrochemical measurements were achieved at room temperature in an aqueous potassium hydroxide (1 M) electrolyte with a three-electrode cell, consisting of a glassy carbon (GC) working electrode, an Ag/AgCl reference electrode (RE), and a Pt-wire counter electrode (CE). Working electrodes were prepared by drop casting the carbon slurry onto the GC electrode. The slurry was prepared by mixing the active material (CB and ACBs) with poly(vinylidene difluoride) (PVDF: average molecular weight 534 000 g mol^{-1}) as the binding agent (5 wt%) in *N*-methyl-2-pyrrolidone (NMP) with a ratio of 95 : 5 (wt; wt) and by ultrasonication until a homogeneous carbon paste was obtained. The carbon paste was spreaded to obtain a thin film which was dried using a vacuum oven for one hour. The conductivity of the electrodes was determined by performing impedance spectroscopy in a frequency range of 10 MHz to 0.1 Hz using a 10 mV excitation signal. Thermogravimetric analysis (TGA) and differential thermogravimetric (DTG) analyses of the ACBs were obtained from a thermogravimetric analyser (PerkinElmer, TGA 4000) available at the Department of Chemical and Process Engineering, University of Peradeniya, Peradeniya, Sri Lanka. The sample was heated from 25 to 1000 °C at the heating rate of 10 °C min^{-1} in the presence of a nitrogen flow rate of 20 ml min^{-1}.

3 Results and discussion

3.1 Functional groups, surface chemistry and yield of CS-based carbon products

3.1.1 Raw CSs and carbonised CBs. FT-IR analyses were performed to determine the structural changes that occurred during the carbonisation and activation process of CB. The resulting spectra for raw CSs exhibit a broad intense peak at 3202 cm^{-1} indicating the O–H stretching vibrations from cellulose, hemicellulose and lignin[31,34] (Fig. 1). The peak at 2928 cm^{-1} corresponds to the C–H stretching vibrations of polysaccharide chain units.[35,36] The C=O stretching from hemicellulose and lignin is indicated by the characteristic peak at 1731 cm^{-1}.[36,37] The asymmetric vibrations of aromatic C=C are indicated by the peaks at 1604 cm^{-1}, and 1510 cm^{-1}, which are obtained for lignin and the characteristic peak obtained for the symmetric C–O–C stretching of cellulose is indicated at 1167 cm^{-1}.[31,36] Therefore, it is confirmed that the raw CSs are composed of cellulose, hemicellulose and lignin. The CS waste biomass usually comprises cellulose, hemicellulose, and lignin.[14,38,39]

As illustrated in Fig. 2 and 3, the FT-IR spectra of all carbonised CB samples indicate the existence of certain common bands corresponding to the functional groups: O–H groups around 3000 cm^{-1} to 3300 cm^{-1}, aliphatic C–H groups around 2800 cm^{-1} to 3000 cm^{-1}, aromatic C=C groups around 1400 cm^{-1} to 1600 cm^{-1}, and C–O–C groups around 1100 cm^{-1} to 1250 cm^{-1}.[36,40,41] However, compared to the FT-IR spectrum of raw CSs, these peaks show weak transmittance, indicating that the carbonised CB samples contain very low concentrations of functional groups.[6,38] Additionally, all carbonised CB samples exhibit similar spectra, suggesting similar structures and functional groups, though the intensity varies depending on the carbonisation conditions applied.

The carbonisation of CSs could be attributed to the breakdown of polymers of cellulose, hemicellulose, and lignin.[14,38,39] Enriching the carbon content and creating the initial porosity in the CS-derived CB are the main purposes of the carbonisation process.[23,42] During the carbonisation, cellulose, hemicellulose, and lignin undergo dehydration, linkage breaking, structural ordering reactions, and finally the polymerisation reactions, which result in a significant amount of volatiles being released

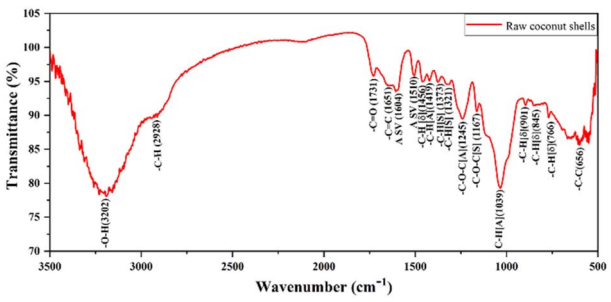

Fig. 1 FT-IR spectrum of raw CSs indicating the presence of functional groups of cellulose, hemicellulose, and lignin.

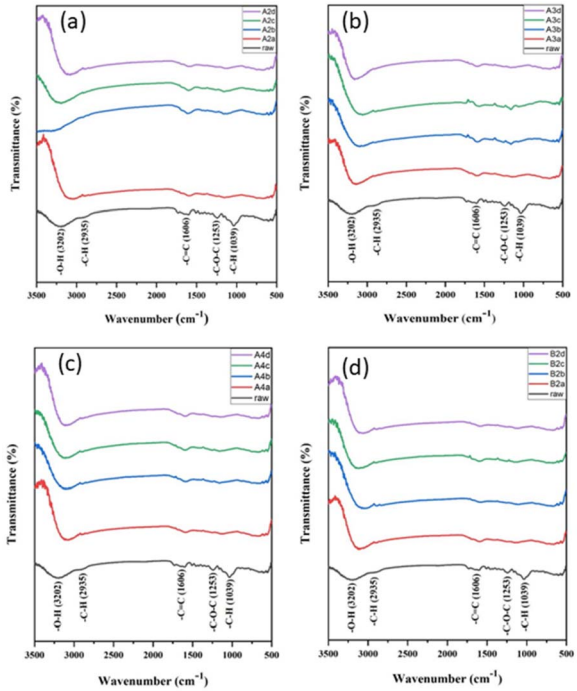

Fig. 2 FT-IR spectra of yielded product at different carbonisation durations. (a) CB carbonised at 450 °C for 2 h, (b) CB carbonised at 450 °C for 3 h, (c) CB carbonised at 450 °C for 4 h, and (d) CB carbonised at 500 °C for 2 h.

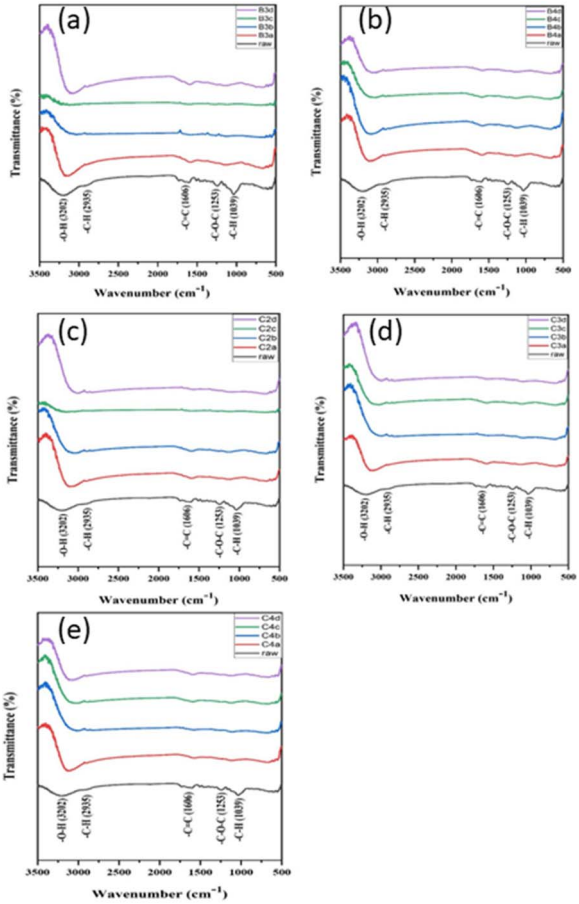

Fig. 3 FT-IR spectra of yielded product at different carbonisation durations. (a) CB carbonised at 500 °C for 3 h, (b) CB carbonised at 500 °C for 4 h, (c) CB carbonised at 550 °C for 2 h, (d) CB carbonised at 550 °C for 3 h, and (e) CB carbonised at 550 °C for 4 h.

from the raw materials and eventually cause pore development.[4,23,43] However, carbonised carbon lacks a well-developed porous structure, making an activation process necessary.

3.1.2 Effect of temperature, time duration, and particle size on the carbonisation process. With increasing temperature, a decrease in the intensities of the FT-IR bands was observed due to the loss of unstable volatiles from the samples. The shift of the O–H band towards a lower wave number and the reduction in its intensity indicate the loss of hydroxyl groups, suggesting enhanced carbonisation and reduced oxygen content.[44] A decrease in the peak intensity of C–H stretching points to the breakdown of aliphatic hydrocarbons. Additionally, the disappearance of the FT-IR band corresponding to the carbonyl stretching indicates alterations in carbonyl-containing functional groups, possibly due to reduction reactions during carbonisation.[32]

As shown in Fig. 2 and 3, all the FT-IR spectra contain a band corresponding to aromatic C=C stretching, indicating the formation of more aromatic structures, signifying higher carbonisation and a more graphitic structure with the increase in temperature.[15,34] Increasing the duration of carbonisation results in a reduction of peak intensities as the longer carbonisation time ensures more conversion of biomass to CB. Additionally, a greater presence of aromatic structures is observed, suggesting increased carbonisation and the development of more graphitic structures.[15,32]

Decreasing particle size in CS samples results in FT-IR spectra showing more intense peaks for O–H groups, likely due to the exposure of more surface hydroxyl groups because of the increased surface area. However, a reduction in the intensities and peak shifts of other bands is observed, which may be attributed to the higher surface area enhancing the reactivity and efficiency of carbonisation, allowing for more uniform heating.[32,44]

Most of the lignocellulose biomass components present in the coconut shells decompose around 550 °C within 2–4 hours, leaving a carbon-rich framework.[6,45,46] Using a higher temperature and extending time duration beyond this may not significantly improve the yield, but could lead to loss of carbon material through volatilisation.[45] Higher temperatures and prolonged heating could degrade the carbon framework causing structural collapse and reducing overall surface area and pore volume.[47] Furthermore, this could promote interaction between inorganic ash components and carbon reducing the quality of the final product.

3.1.3 Yield of CB after the carbonisation process. After the carbonisation process of CS (10 g) samples, as illustrated in Fig. 4, the maximum yield of 3.801 g was obtained for the CB sample A2c. The minimum yields of 0.846 g and 0.872 g were obtained for the CB samples A3b and C3c respectively. The

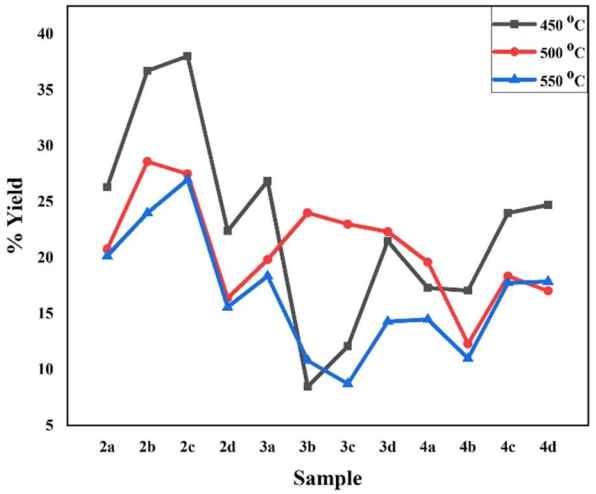

Fig. 4 CB yields after the carbonisation process showing the effect of different carbonisation parameters on CB yield.

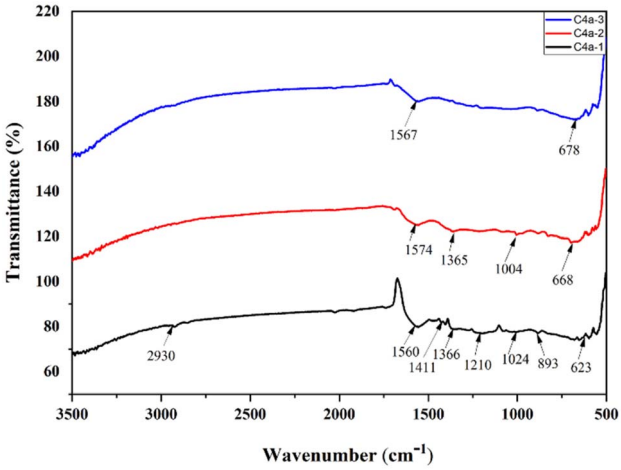

Fig. 5 FT-IR spectrum of ACB indicating the presence of aromatic structures and other functional groups in ACB.

carbonisation experiments were performed in multiple trials and the average value was used for each sample. It was given in a previous study that the maximum yield of 9.04 g for the CS-based CB was obtained for the carbonisation temperature of 280 °C and the minimum yield of 6.78 g was attained for the carbonisation temperature of 420 °C.[48] Furthermore, there is a reduction in the yields of CB samples when increasing carbonisation temperature and duration of carbonisation, confirming that higher temperatures and higher carbonisation durations enhance the carbonisation process by removing more volatiles from the CB samples.

3.1.4 CS-based ACBs. A systematic evaluation of all 36 CB samples was carried out to identify the most appropriate sample for alkali treatment. The selection was based on a balance between the structural quality (carbonisation) and process efficiency (material yield). FTIR spectroscopy was first employed to evaluate structural quality, whereby the sample exhibiting the most substantial suppression of oxygen-containing functional groups and the highest degree of graphitic ordering was identified. In addition, carbonisation yield was measured for all 36 CB samples, as illustrated in Fig. 4. The yields ranged from 3.801 g to 0.846 g, showing the variations in carbon retention. Generally, higher yields indicate incomplete carbonisation, while the lowest yields correspond to low carbon recovery, with higher ash and structural degradation. Sample C4a exhibited a yield of 1.450 g, which falls within the optimal mid-range, indicating adequate carbonisation while maintaining practical material recovery for subsequent activation. Based on its favourable FTIR features and acceptable yield, C4a was selected for KOH treatment. After selecting this sample, SEM-EDS, XRD, and EIS analyses were performed and compared with the other ACB samples to further validate its structural integrity and elemental composition.

Fig. 5 shows the FT-IR spectrums of ACBs prepared with different weight ratios of KOH. The presence of a sharp peak in the FT-IR spectrum for the C=C aromatic ring stretching at 1567 cm^{-1} for all the ACB samples indicates the presence of a graphitic crystalline nature after the treatment with different weight ratios of KOH.[15,49,50] Specifically, the FT-IR spectra of ACB formed with a CB : KOH ratio 1 : 2 show a small intense peak at 2930 cm^{-1}, corresponding to the C–H stretching and the presence of C–H stretching bands at 1365 cm^{-1} and C–O–C stretching bonds denote at 1210 cm^{-1} in the FT-IR pattern suggests the presence of alkane, alkene, and ketone/aldehyde groups in the structure.[51–53] Moreover, the spectra for ACB formed with CB : KOH ratios of 1 : 2 and 1 : 4 display the formation of characteristic peaks for ether and ester groups after the treatment with KOH.[4,51] As illustrated in Fig. 5 the purity of the ACB increases with the increase of KOH concentration as the intensity of the peaks reduces when increasing KOH.[6,15] However, it reduces the graphitic crystalline nature when the excess of KOH is used for the activation. During activation, impregnating CB with a strong base like KOH facilitates the removal of hydroxyl groups from the carbon structure and promotes the formation of oxygen-containing functional groups on the surface of the activated carbon. Moreover, KOH reacts with the carbon material to form various potassium compounds (K_2CO_3, K_2O) and gases (H_2, CO), which etch the carbon matrix and create a porous structure.[14,54] However, higher temperatures cause KOH to become excessively reactive, which might harm the carbon structure by causing excessive gas evolution and possibly over-etching.[55] Higher temperatures might sometimes cause pores to overdevelop, resulting in overly large or collapsed structures.[56,57] At 120 °C KOH does not strongly activate the carbon, instead, it chemically modifies the surface, adding functional groups including OH and COOH that enhance the dispersibility in toner formulation. Excessive porosity and pore collapse are unnecessary for toner application that requires dense particulates.

The effectiveness of activated carbon derived from various high-carbon content sources largely depends on this activation process.[10] The primary goal of activation is to transform CB into ACB with enhanced porosity by removing ash and uncarbonated

biomass. This process also aims to introduce some structural ordering, resulting in a highly porous solid with a large surface area as the final product.[58] This enhancement of porosity and surface area is achieved by three steps. First, opening previously inaccessible pores; second, creating new pores by deep penetration of the activating agent; and lastly widening the existing pores.[6,53]

3.2 Surface morphologies and elemental composition of CS-based CBs and ACBs

The SEM results revealed the successful completion of the activation process of CB using the KOH activator (Fig. 6). However, significant differences between the surface morphology of carbonised CB and activated CB samples with different KOH ratios were observed. The impregnation of CB with KOH produced a smooth surface of ACB with numerous micropores opening and well-developed porosity compared to the carbonised CB sample.[59] As shown in Fig. 6(a), the surface of the carbonised CS sample at 550 °C was rough and with no pores available on the surface. Chemical treatment with KOH caused the existence of perfect pores which are distributed randomly on the ACB surface.[31,60] As shown in Fig. 6(b) and (c), pores are quite spherical and well-structured with clear openings producing a large surface area.

Moreover, the SEM image analyses clearly show that increasing KOH concentration causes an increase in the pore number and pore size of ACB.[61,62] The pores in the ACB exhibit a wider opening, which could be attributed to an excessive chemical attack, causing the reduction of more carbon content as CO_2 from the surface of CS-based CB. This will cause the loss of high-strength carbon from CB which causes the reduction of the final yield of ACB and the reduction of quality of the ACB as a black colourant in toner powder production. However, pores tend to be much smaller as further increases in KOH concentration due to the carbon collapsing.[49,62] As illustrated in Fig. 6(b)–(d), activation with KOH not only induces a microporous structure in ACB but also weakens and gradually deteriorates the internal carbon structure when applied excessively.

As illustrated in Fig. 6(b) and (c), the ACB produced by CB to KOH weight ratios 1 : 2 and 1 : 4 (C4a-1 and C4a-2) exhibits well-spherical micropores with an average pore size of 0.343 μm and 0.656 μm respectively, resulting in a high surface area providing more surface to attach properly with the binder polymers and other additives in the synthesis process of electromagnetic toner powders. The microporous structure increases the surface area available for interactions with the additives of the toner, provides more sites for the attachment, and ensures the uniform distribution of the components in the toner powders. However, ACB produced with a 1 : 4 weight ratio (C4a-2) exhibits larger micropores compared to the ACB produced by a 1 : 2 weight ratio (C4a-1), possibly due to the high amount of KOH leading to more aggressive etching and removal of more carbon from the CB surface.[58,61] This aggressive etching increases the pore size but reduces the quality of the ACB as a black colourant due to the reduced density of carbon and larger pores may lead to a less intense black colour. Also, ACBs produced by a 1 : 6 weight ratio (C4a-3), exhibit very small micropores with an average pore size of 0.236 μm and show the potential carbon collapse, due to the excessive etching by KOH, suggesting that lower KOH concentrations (such as CB to KOH weight ratio 1 : 2) enhance the surface area while maintaining the overall performance of ACB.

In order to determine the suitability of ACB samples for toner powder formulations, particle size analysis was carried out by using SEM to obtain high-resolution images followed by the quantitative measurement using ImageJ software. Fig. 7 shows the histogram and the corresponding fitted distribution curve for the particle size distribution of the ACB samples. The majority of the ACB particles were concentrated in the range of 10–20 μm with a mean size of 21.39 μm, indicating a skewed particle size distribution. Generally, toner powders with narrow size distribution and small particle sizes are necessary to achieve high-resolution images.[63] For high-resolution printing applications, toner powders should typically have an average particle size of 10–15 μm.[63–65] As shown in the figure most of the

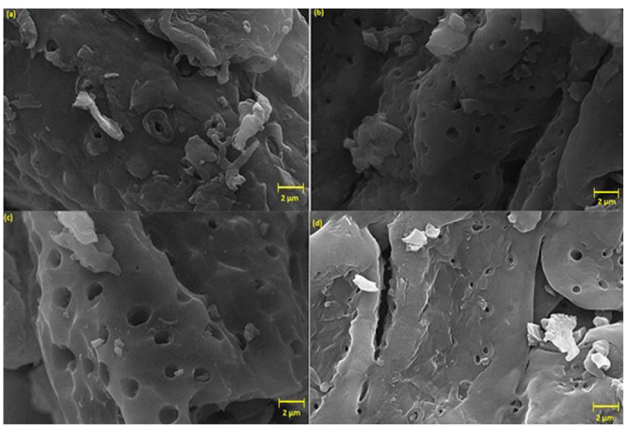

Fig. 6 SEM images of (a) carbonised CS sample at 550 °C (b) ACB produced with CB : KOH ratio 1 : 2 (c) ACB produced with CB : KOH ratio 1 : 4 (d) ACB produced with CB : KOH ratio 1 : 6.

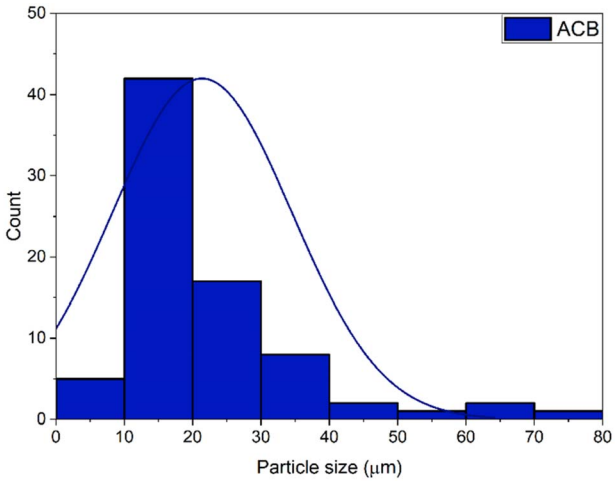

Fig. 7 Histogram and the fitted distribution curve for the particle size distribution of ACB samples.

synthesised ACB particles lie within the acceptable size range for toner powders, however, the broad size distribution observed in the sample with few large particles of 80 μm may lead to challenges in achieving uniform charge distribution and print quality.[66] Further milling and sieving to remove oversized particles could enhance the uniformity of the samples.

To determine the changes in the elemental components before and after carbonisation and CB activation, the Energy Dispersive X-ray Spectroscopic (EDS) analysis was performed. The results illustrated in Fig. 8 and 9 revealed that raw CSs, carbonised CB, and ACBs contain different contents of carbon and oxygen elements. As presented in Table 2 raw CSs contain only about 50 wt% of carbon which is consistent with the values reported in the literature.[67] The carbonised CSs exhibited the highest carbon weight concentration of 72.8 wt% and the lowest oxygen concentration of 12.3 wt%, making them the most suitable material for the synthesis of toner powders. After the treatment with KOH, the amount of carbon reduced due to the release of volatiles while the amount of oxygen increased due to the introduction of oxygen-containing functional groups. Comparatively, C4a-1 showed a relatively high carbon content of 69.2 wt% and 22.5 wt% of oxygen making it the best among the ACB samples for the synthesis of toner powders. The higher carbon content ensures excellent black pigmentation and electrical conductivity of the toner powders while higher oxygen content will reduce the thermal stability and electrical conductivity of the conductive toner powders. Additionally, the presence of Au and Pd peaks in the EDS spectra indicated the external contamination resulting from the coating techniques, which was a sample preparation artefact. The presence of K and Cl peaks in the spectrum was likely due to the chemical treatment of KOH during the activation and HCl during the subsequent cleaning steps. However, K and Cl are also inherent elements naturally present in raw CSs.[28,55]

3.3 Crystallographic structure of raw CSs, CBs, and ACBs

The XRD analysis of raw CSs revealed that they are primarily composed of cellulose and inorganic minerals such as $CaCO_3$ and SiO_2.[68,69] As illustrated in Fig. 10 the XRD pattern of raw CSs

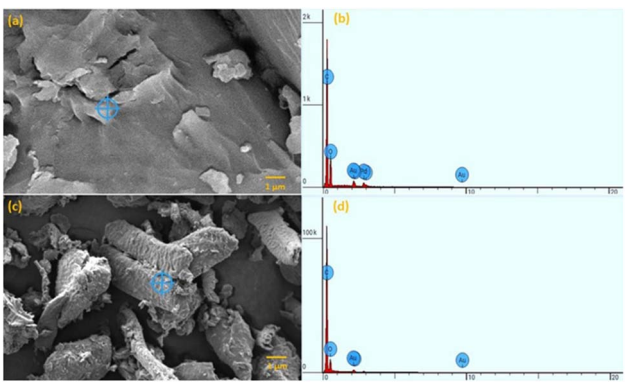

Fig. 8 SEM and EDS images of (a and b) raw CSs and (c and d) carbonised CB samples indicating the changes in elemental composition before and after carbonisation.

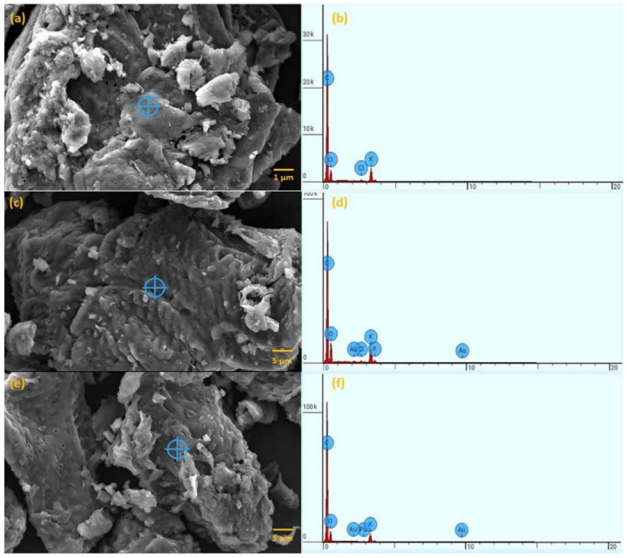

Fig. 9 SEM and EDS images indicating the difference in composition of elements including carbon and oxygen of the synthesised ACB samples (a and b) C4a-1, (c and d) C4a-2, (e and f) C4a-3.

exhibits an intense peak at around $2\theta = 22.70°$ bearing *hkl* value (002) and less intense peaks located at $2\theta = 16.42°$, and 34.64° bearing *hkl* values (101), and (222) respectively, confirming the presence of high content of carbon. Also, few intense peaks were observed for the $CaCO_3$ and SiO_2 which are naturally contained in the CSs.[68]

The XRD pattern depicted in Fig. 11 for the CS-derived CB (C4a) shows two broad peaks located at $2\theta = 23.18°$, and 47.09° indicating the formation of carbon-like structures in the *hkl* plane of (002), and (101) confirming the formation of amorphous phase.[70,71] The alkali treatment using KOH caused the formation of both amorphous and crystalline phases within CB samples. As shown in Fig. 12 increase in KOH concentration resulted in an increase in the microcrystalline nature of CB causing sharp peaks in the XRD pattern. The amorphous form of CB consists of carbon atoms arranged randomly, lacking a well-defined crystalline structure.[49,72] Additionally, amorphous carbon contains heteroatoms and various impurities, contributing to its disordered structure. As the KOH concentration increases, the structure does not fully transform into a graphitic form. However, there is a noticeable presence of

Table 2 Elemental composition of raw CSs, CB and ACB samples analysed by EDS

	Atomic concentration (%)		Weight concentration (%)	
Sample type	Carbon	Oxygen	Carbon	Oxygen
Raw CSs	67.489	30.091	50.000	29.700
Carbonised CSs	87.774	11.132	72.800	12.300
C4a-1	79.913	19.504	69.200	22.500
C4a-2	68.276	25.992	55.800	28.300
C4a-3	77.453	19.179	67.600	22.300

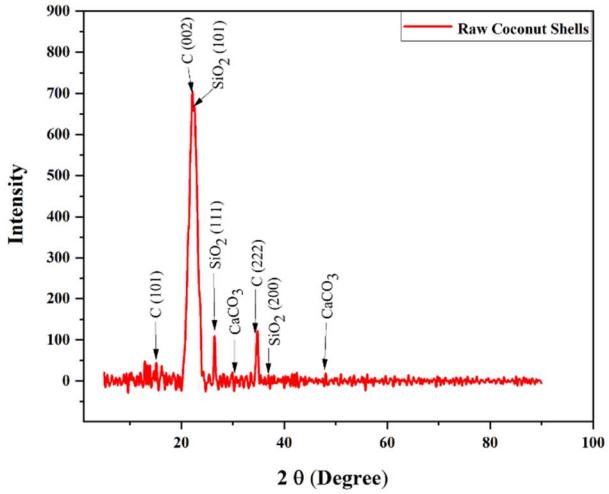

Fig. 10 XRD pattern for raw CSs indicating the presence of cellulose, $CaCO_3$, and SiO_2 as major constituents in raw CS.

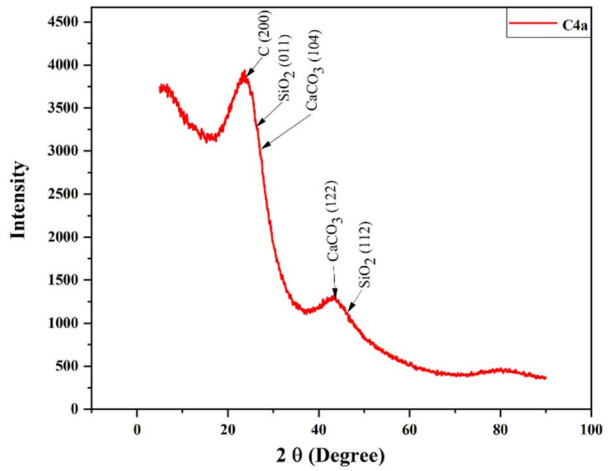

Fig. 11 XRD pattern for CB sample carbonised at 550 °C for 4 h showing corresponding peaks for amorphous carbon, $CaCO_3$, and SiO_2.

microcrystallinity in sample C4a-2, which the incorporated impurities could induce during the activation process.[57] The sharp peaks in the diffraction pattern reflect the observed microcrystallinity. These impurities may act as nucleation sites and promote the formation of tiny crystallites without appreciably enhancing the overall structural ordering towards a fully graphitic state. Although this microcrystallinity indicates a certain level of short-range order, it does not enhance the electrical conductivity or thermal stability of ACBs. Rather, the impurities and the associated microcrystallites add to structural heterogeneity, which may affect the overall properties of the ACBs but does not always make them better for practical applications like conductive materials or toner powders. However, there is a notable similarity between the XRD patterns of the samples C4a-1 and C4a-3 having the amorphous carbon structure. Additionally, the XRD patterns of these ACBs

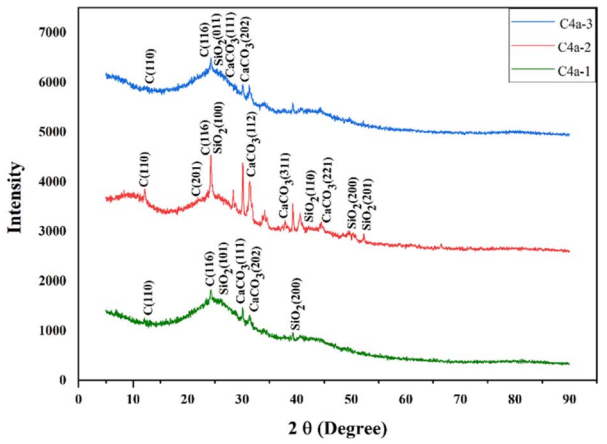

Fig. 12 XRD pattern for CS-based ACB samples showing both amorphous and crystalline structure.

prepared in this study show some similarity to those reported in a previous investigation.[12]

3.4 Electrochemical behaviour of CBs and ACBs

The Electrochemical Impedance Spectroscopy (EIS) data of CB (C4a) and ACB (C4a-1, C4a-2, and C4a-3) samples offer vital information about their electrical characteristics which are essential for evaluating their suitability for conductive toner powder applications. Fig. 13 shows the Nyquist plot for CB samples, the real part of the impedance (Z') is plotted against the imaginary part (Z'') and the equivalent circuit which was constructed based on the circuit used in a previous study.[73] In general, Nyquist plots consisted of one or two high-frequency semicircular region(s) corresponding to charge transfer processes and a low-frequency linear region related to diffusion limitations and porosity/roughness in the carbon materials.[33] For the investigated samples Nyquist presents a semicircle in the high-frequency region and a linear relationship in the mid-frequency and low-frequency range, with the diameter of the

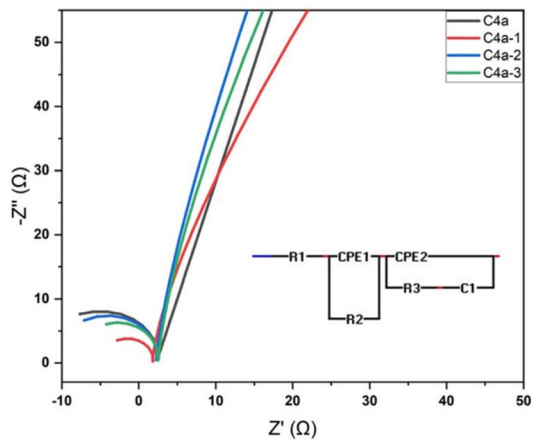

Fig. 13 Nyquist diagram of CB and ACB samples synthesised with different KOH concentrations. The inset picture shows the electrical circuit analogue of the EIS curve.

semicircle related to the charge transfer resistance (R_{ct}), the intersection of the semicircle to the *Z*-axis representing the bulk resistance (R_s), and the straight line related to the capacitive behaviour.[74–76]

As shown in Fig. 13 the curves for C4a-1 and C4a-3 exhibit smaller semicircles in the high-frequency region, corresponding to lower charge transfer resistance. In contrast, the curve for C4a-2 shows a larger semicircle, reflecting its poor electrical conductivity. Additionally, the steeper incline in the low-frequency region for C4a-1 suggests enhanced capacitive behaviour and efficient charge storage. This trend was supported by the resistance and capacitance values obtained from the fitted equivalent circuit given in Fig. 13, which includes bulk resistance (R_s), charge transfer resistance (R_{ct}), double layer capacitance (C) and constant phase elements (CPE).[73] The circuit element values are summarized in Table 3. As indicated in Table 3, C4a-1 shows the lowest R_s (4.7805 Ω) and R_{ct} (6.4769 Ω) compared to the carbonised CB sample (7.1209 Ω and 9.7435 Ω, respectively) and the other ACB samples. This suggests that C4a-1 has the lowest overall resistance and improved charge conduction pathways, both of which are essential for enhancing toner powder conductivity. Furthermore, C4a demonstrate the highest capacitance (54.136 10^{-6} F) but it has a much higher R_s compared to C4a-1. The highest R_s of 10.443 Ω was shown by C4a-2 indicating the lowest conductivity while the sample C4a-3 showed a moderate R_s of 6.9694 Ω.

In two-component magnetic toner systems, the higher conductivity of the CB enables more effective charge exchange between the toner particles and the carrier, resulting in faster and more stable triboelectric charging.[77] Such stability during printing supports a consistent charge-to-mass ratio (Q/M), which affects image density, edge sharpness, and background cleanliness. The C4a-1, having the lowest R_{ct} and R_s with improved electrical characteristics, has practical implications for toner performance. Conversely, samples with higher resistance (C4a-2) are likely to exhibit slower charge relaxation and reduced charge mobility, which can cause insufficient charging, toner over-development, or fogging. Therefore, the superior conductivity and capacitive behaviour of C4a-1 suggest that it would provide more reliable charge control and potentially enhance print quality in real toner formulations. Although full printer-level evaluation is beyond the scope of this study, the EIS results strongly indicate that C4a-1 possesses the most favourable electrochemical characteristics for high-performance toner applications.

Table 3 Resistance and capacitance values obtained from the fitted equivalent circuit analogue of EIS curves

Sample	Bulk resistance/Ω	Charge transfer resistance/Ω	Capacitance/10^{-6} F
C4a	07.121	09.743	54.14
C4a-1	04.781	06.477	52.55
C4a-2	10.443	12.627	39.80
C4a-3	06.969	09.992	47.20

Although the EIS measurements were conducted in an aqueous 1 M KOH electrolyte using a three-electrode configuration, and therefore do not represent the dry-state behaviour of the toner powders, EIS still provides a comparative indication of the intrinsic electron-transfer capability of each ACB sample. The absolute values of R_s and R_{ct} obtained in the liquid phase cannot be directly translated to toner performance parameters such as charge acceptance, triboelectric charging, or powder conductivity. However, the EIS results provide a clear comparison of the ACB samples concerning their intrinsic electron-transfer capability, allowing differentiation of their relative conductivity trends. These trends are consistent with the structural variations revealed by FTIR, XRD and SEM analyses. The structural differences, such as graphitisation degree, defect reduction, and porosity, are known to influence dry-state charge transport in toner additives. Furthermore, the charge transfer resistance R_{ct} is a measure of the kinetic barrier to charge exchange at the material interface. The C4a-1, having the lowest R_s and R_{ct} values, indicates a superior intrinsic electronic network and interface accessibility.[78,79] This superior intrinsic efficiency is the core parameter ruling the effectiveness of the ACB in forming a highly conductive percolation pathway within the dry polymer matrix, essential for uniform charge acceptance and control in the toner system.[80] Thus, despite the environmental differences, the EIS analysis offers supportive evidence that C4a-1 has inherently superior charge-transport characteristics compared to the other samples, making it the most promising candidate for conductive toner formulations.

3.5 Thermal stability of ACBs

TGA and DTG analyses were performed aiming to evaluate the thermal stability of ACB samples. Fig. 14 and 15 show the TGA and DTG curves for the ACB samples C4a-1 and C4a-2 respectively. As shown in the figures the initial weight loss for both samples around 90–100 °C corresponds to the evaporation of adsorbed moisture or removal of loosely bound volatile substances, which is typical for materials with porous structures.[37,81] Furthermore, C4a-2 exhibits a noticeable weight loss

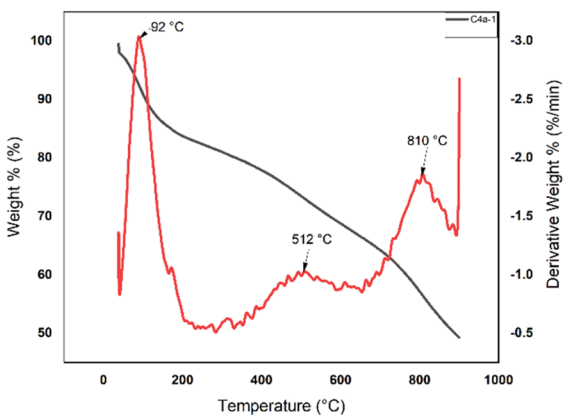

Fig. 14 TGA and DTG curves of C4a-1 produced by CB to KOH weight ratios 1 : 2 showing different decomposition stages at different temperatures.

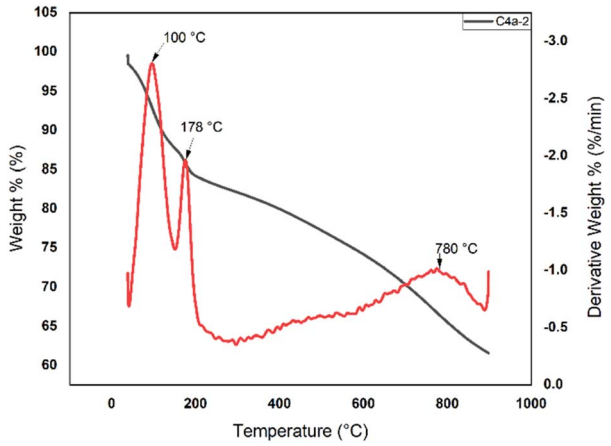

Fig. 15 TGA and DTG curves of C4a-2 produced by CB to KOH weight ratios 1 : 4 showing different decomposition stages at different temperatures.

at 178 °C indicating the removal of volatile organic components and a larger weight loss than the sample C4a-1. The flowability, storage stability, and printing effectiveness of the toner powders could be impacted by moisture and volatiles. Consequently, pre-drying ACBs at this temperature might ensure a reliable starting material.

Both ACB samples were thermally stable up to 400 °C, which is well within the range of toner processing and printing, and the stable region of both samples from 100 to 400 °C indicates that no significant decomposition occurs within this range. A noticeable drop in weight was observed from 400–900 °C for both samples indicating the decomposition of organic compounds or carbon oxidation.[37,55,82] The DTG curves demonstrated that the secondary decomposition peak for C4a-1 was detected at approximately 512 °C, while the peak corresponding to the combustion of the residual carbon was detected at around 810 °C. Around 780 °C, a secondary decomposition peak was observed for sample C4a-2, suggesting carbon combustion or structural degradation. Additionally, the residual mass for C4a-1 and C4a-2 at 900 °C was approximately 55% and 60%, respectively, suggesting that the latter sample had higher ash content or inorganic contaminants. For toner applications, a low impurity level is preferred since a higher ash or impurity content could interfere with charge control or result in printing defects.

3.6 Potential as a black colourant in printing applications

Based on the above results, ACB is primarily composed of carbon with minor amounts of oxygen and hydrogen with a highly porous structure due to the activation of KOH. The synthesised ACB was typically a deep black colour, which was due to the high carbon content and fine particulate nature of the material which makes it an excellent black colourant providing dark and rich prints in various printing applications.[83] Carbonisation of 0.1 mm CS particles at 550 °C for 4 h ensured complete carbonisation, resulting the formation of fine carbon particles with deep black colouration while lower carbonisation temperatures and durations caused less intense black colouration. Carbonisation at 550 °C caused less graphitic but conductive amorphous carbon structure whereas prolonged carbonisation may overly oxidise or degrade carbon affecting its colour intensity and uniformity. Furthermore, low-temperature KOH treatment at 120 °C caused ACB with a smooth surface and moderate functionalisation which may result in better dispersion in polymer matrices during toner preparation.

Generally, good colour tinting needs CB with low structure and high surface area or smaller particle size.[29,84] The ACB synthesised with CB : KOH weight ratio 1 : 2 and 1 : 4 (C4a-1 and C4a-2 respectively) contains a high surface area with a highly porous structure with an average pore size of 0.343 μm and 0.656 μm. Furthermore, most of the synthesised ACB particles lie within the acceptable size range (10–15 μm) for toner powders. The fine particle size and the large surface area provide more surface to attach properly with the binder polymers and other additives allowing good dispersion in various printing formulations, ensuring uniform colour and print quality. However, C4a-1 showed a relatively high carbon content of 69.2 wt% making it the best among the ACB samples for the synthesis of toner powders. The higher carbon content ensures excellent black pigmentation and electrical conductivity of the toner powders while the higher oxygen content of C4a-2 could potentially reduce the thermal stability and electrical conductivity of the conductive toner powders.

Moreover, EIS data reveals that sample C4a-1 has the lowest overall resistance hence the highest charge conduction pathway, both of which are essential for its utility as a conductive material in the synthesis of toner powders. Based on the TGA results, both ACB samples (C4a-1 and C4a-2) were thermally stable up to 400 °C, which is well within the range of toner processing and printing. However, sample C4a-1 shows low moisture, low volatile content, and simpler decomposition behaviour with fewer distinct peaks in the DTG curve suggesting fewer surface functional groups. Furthermore, TGA curves showed that the residual mass of C4a-2 was higher than C4a-1 at 900 °C, indicating that C4a-2 contains more ash or inorganic impurities that might interfere with charge control or result in printing flaws. Consequently, C4a-1 is the most promising option for toner powder production since it can serve as both a black colourant and an electrically conductive material in toner powders.

Although full toner-level performance evaluations such as optical density, colourimetric response, polymer dispersibility, triboelectric charging behaviour, and print quality analysis, were beyond the scope of this work, the extensive material-level characterisation conducted through FTIR, SEM, EDS, XRD, TGA, and EIS has provided critical insight into key properties governing toner functionality. These analyses elucidated the influence of surface chemistry, particle morphology, porosity, thermal stability, and intrinsic electrical conductivity on the suitability of CS-derived ACB for electrically conductive toner applications. Collectively, the results enabled the identification of the most promising ACB candidate for future toner formulation studies. This work therefore establishes a robust foundational framework for subsequent investigations into toner

processing, formulation optimisation, and full-scale electrophotographic printing performance.

4 Conclusions

Synthesis of ACBs from CS waste using KOH treatment and optimised carbonisation conditions was successfully attained, highlighting their potential as a black colourant in the electrically conductive toner powder industry. This process could offer significant enhancements in developing toner powders, improving their conductivity and print quality. The optimised sample, C4a-1 (CB to KOH ratio 1 : 2), exhibited ideal characteristics for conductive toner applications, including a high carbon content (69.2 wt%), excellent black pigmentation, and low resistance. Moreover, fine particle size (10–15 μm) and porous structure with higher surface area may ensure good dispersion in polymer matrices and proper binding with additives, facilitating uniform colour and print quality. Also, thermal stability up to 400 °C, low moisture and ash content, and simpler decomposition behaviour of C4a-1 make it an ideal material for a black colourant in toner powders. In contrast, the printing performance of the toners may be affected by the increased oxygen and ash content, larger pores, and decreased electrical conductivity of C4a-2, whereas C4a-3 exhibited mild resistance and smaller pores associated with carbon collapse. In conclusion, C4a-1 was the best option for being used as a black colourant and conductive agent in toner powders, providing insights into the synthesis of CS-based ACBs as a potential black colourant in electrically conductive toner powder production.

Conflicts of interest

There are no conflicts of interests to declare.

Data availability

All data generated or analysed during this study are fully included within the submitted manuscript. No separate datasets or supplementary data files are available for submission.

Acknowledgements

The authors gratefully acknowledge the financial support provided by the National Research Council, Sri Lanka through the research grant under contact number 22/127. Also, we are grateful for the laboratory support for XRD analysis from Surface and Material Science core labs, KUAST, Abu Dhabi, UAE.

References

1 R. G. Karmankar, Extraction of carbon black from coconut shell, *Int. Res. J. Eng. Technol.*, 2016, **3**(1), 1286–1291.
2 M. Singh and R. L. Vander Wal, Nanostructure Quantification of Carbon Blacks, *J. Carbon Res.*, 2018, **5**(1), 2, DOI: 10.3390/c5010002.
3 Y. Fan, G. D. Fowler and C. Norris, Potential of a Pyrolytic Coconut Shell as a Sustainable Biofiller for Styrene-Butadiene Rubber, *Ind. Eng. Chem. Res.*, 2017, **56**(16), 4779–4791, DOI: 10.1021/acs.iecr.7b00405.
4 C. Jiang, J. Bo, X. Xiao, S. Zhang, Z. Wang, G. Yan, Y. Wu, C. Wong and H. He, Converting waste lignin into nanobiochar as a renewable substitute of carbon black for reinforcing styrene-butadiene rubber, *Waste Manag.*, 2020, **102**, 732–742, DOI: 10.1016/j.wasman.2019.11.019.
5 H. P. S. A. Khalil, P. Firoozian, I. O. Bakare, H. Akil and A. Noor, Exploring biomass based carbon black as filler in epoxy composites: Flexural and thermal properties, *Mater. Des.*, 2010, **31**(7), 3419–3425, DOI: 10.1016/j.matdes.2010.01.044.
6 H. K. Yağmur and İ. Kaya, Synthesis and characterization of magnetic ZnCl2-activated carbon produced from coconut shell for the adsorption of methylene blue, *J. Mol. Struct.*, 2021, **1232**, DOI: 10.1016/j.molstruc.2021.130071.
7 A. A. Ceyhan, Ö. Şahin, C. Saka and A. Yalçin, A novel thermal process for activated carbon production from the vetch biomass with air at low temperature by two-stage procedure, *J. Anal. Appl. Pyrolysis*, 2013, **104**, 170–175.
8 U. D. Hamza, N. S. Nasri, N. A. S Amin, J. Mohammed and H. M. Zain, Characteristics of oil palm shell biochar and activated carbon prepared at different carbonization times, *Desalin. Water Treat.*, 2016, **57**(17), 7999–8006, DOI: 10.1080/19443994.2015.1042068.
9 D. Das, D. P. Samal and M. BC, Preparation of Activated Carbon from Green Coconut Shell and its Characterization, *J. Chem. Eng. Process Technol.*, 2015, **06**(05), DOI: 10.4172/2157-7048.1000248.
10 E. A. Saputro, V. Dwi, R. Wulan, B. Y. Winata, R. Ramadhan and N. K. Erliyanti, Review article The Process of Activated Carbon from Coconut Shells Through Chemical Activation, *J. Sci. Technol.*, 2020, **09**, DOI: 10.22487/25411969.2019.v9.i1.15042.
11 M. A. Suryawanshi, A. Bandgar, C. Mhaske and S. Shetty, Production of activated carbon from various natural resources and its application, *J. Emerg. Technol. Innov. Res.*, 2020, **7**(9), 560–565.
12 A. I. Bakti, P. L. Gareso and N. Rauf, Characterization of Active Carbon from Coconut Shell using X-Ray Diffraction (X-RD) and SEM-EDX Techniques, *J. Penelit. Fis. Apl.*, 2018, **8**(2), 115, DOI: 10.26740/jpfa.v8n2.p115-122.
13 F. Destyorini, Y. Irmawati, A. Hardiansyah, H. Widodo, I. N. D. Yahya, N. Indayaningsih, R. Yudianti, Y. I. Hsu and H. Uyama, Formation of nanostructured graphitic carbon from coconut waste via low-temperature catalytic graphitisation, *Eng. Sci. Technol. Int. J.*, 2021, **24**(2), 514–523, DOI: 10.1016/j.jestch.2020.06.011.
14 A. Ajien, J. Idris, N. Md Sofwan, R. Husen and H. Seli, Coconut shell and husk biochar: A review of production and activation technology, economic, financial aspect and application, *Waste Manag. Res.*, 2023, **41**(1), 37–51, DOI: 10.1177/0734242X221127167.
15 M. J. Rampe, I. R. S. Santoso, H. L. Rampe, V. A. Tiwow and A. Apita, Infrared Spectra Patterns of Coconut Shell Charcoal

as Result of Pyrolysis and Acid Activation Origin of Sulawesi , Indonesia, *E3S Web Conf.*, 2021, **328**, 08008, DOI: 10.1051/e3sconf/202132808008.

16 N. Arena, J. Lee and R. Clift, Life Cycle Assessment of activated carbon production from coconut shells, *J. Clean. Prod.*, 2016, **125**, 68–77, DOI: 10.1016/j.jclepro.2016.03.073.

17 S. D. Lakshmi, P. K. Avti and G. Hegde, Activated carbon nanoparticles from biowaste as new generation antimicrobial agents: A review, *Nano-Struct. Nano-Objects*, 2018, **16**, 306–321, DOI: 10.1016/j.nanoso.2018.08.001.

18 E. H. Sujiono, D. Zabrian, M. Zurnansyah, V. Zharvan, Samnur and N. A. Humairah, Fabrication and characterization of coconut shell activated carbon using variation chemical activation for wastewater treatment application, *Results Chem.*, 2022, **4**, 100291, DOI: 10.1016/j.rechem.2022.100291.

19 R. G. Karmankar, Extraction of carbon black from the coconut shell, *Int. Res. J. Eng. Technol.*, 2018, **3**(01).

20 J. Lee, A. K. Sarmah and E. E. Kwon, Production and formation of biochar, *Biochar from Biomass Waste*, ed. Y. S. Ok, D. C. W. Tsang, N. Bolan and J. M. Novak, Elsevier, 2018, pp. 3–18, DOI: 10.1016/B978-0-12-811729-3.00001-7.

21 R. Narzari, N. Bordoloi, R. S. Chutia, N. Gogoi, A. Bora and R. Kataki, Biochar: An Overview on its Production, Properties and Potential Benefits, in *Biol. Biotechnol. Sustain. Dev.*, ed. H. Choudhury, Research India Publications, New Delhi, 2015, pp. 13–40, DOI: 10.13140/RG.2.1.3966.2560.

22 M. H. Samsudin, M. A. Hassan, J. Idris, N. Ramli, M. Z. Mohd Yusoff, I. Ibrahim, M. R. Othman, A. A. Mohd Ali and Y. Shirai, A one-step self-sustained low temperature carbonization of coconut shell biomass produced a high specific surface area biochar-derived nano-adsorbent, *Waste Manag. Res.*, 2019, **37**(5), 551–555, DOI: 10.1177/0734242X18823953.

23 W. Li, K. Yang, J. Peng, L. Zhang, S. Guo and H. Xia, Effects of carbonization temperatures on characteristics of porosity in coconut shell chars and activated carbons derived from carbonized coconut shell chars, *Ind. Crops Prod.*, 2008, **8**, 190–198, DOI: 10.1016/j.indcrop.2008.02.012.

24 A. H. Jawad, S. Sabar, M. A. M. Ishak, L. D. Wilson, S. S. Ahmad Norrahma, M. K. Talari and A. M. Farhan, Microwave-assisted preparation of mesoporous-activated carbon from coconut (Cocos nucifera) leaf by H_3PO_4 activation for methylene blue adsorption, *Chem. Eng. Commun.*, 2017, **204**(10), 1143–1156, DOI: 10.1080/00986445.2017.1347565.

25 M. M. A. Daouda, A. V. O. Akowanou, S. E. R. Mahunon, C. K. Adjinda, M. P. Aina and P. Drogui, Optimal removal of diclofenac and amoxicillin by activated carbon prepared from coconut shell through response surface methodology, *S. Afr. J. Chem. Eng.*, 2021, **38**, 78–89, DOI: 10.1016/j.sajce.2021.08.004.

26 L. Wang, Y. Ma, H. Liu, Y. Guo, B. Yang and B. Chang, Leveraging porosity and morphology in hierarchically porous carbon microtubes for CO_2 capture and separation from humid flue gases, *Sep. Purif. Technol.*, 2025, **354**, 128910, DOI: 10.1016/j.seppur.2024.128910.

27 W. Shi and Y. Guo, Dynamic tailoring of the gradient porosity of biomass-derived porous carbons for highly effective CO2 capture, *Green Chem.*, 2025, **27**, 11416–11428, DOI: 10.1039/d5gc03217b.

28 Z. U. Nisa, L. K. Chuan, B. H. Guan, F. Ahmad and S. Ayub, A Comparative Study on the Crystalline and Surface Properties of Carbonized Mesoporous Coconut Shell Chars, *Sustain*, 2023, **15**(8), 1–15, DOI: 10.3390/su15086464.

29 M. Ataeefard, Production of black toner through emulsion aggregation of magnetite, carbon black, and styrene-acrylic co-polymer: Investigation on the effect of variation in components, *J. Compos. Mater.*, 2015, **49**(13), 1553–1561, DOI: 10.1177/0021998314536069.

30 H. Liu, S. Wen, J. Wang and Y. Zhu, Preparation and Characterization of Carbon Black- Polystyrene Composite Particles by High-Speed Homogenization Assisted Suspension Polymerization, *J. Appl. Polym. Sci.*, 2012, **123**, 3255–3260.

31 N. A. Anuwar and P. F. M. Khamaruddin, Optimization of Chemical Activation Conditions for Activated Carbon From Coconut Shell Using Response Surface Methodology (RSM) and Its Ability to Adsorb CO_2, in *Proc. Third Int. Conf. Sep. Technol. (ICoST 2020)*, 2021, pp. 234–248, DOI: 10.2991/aer.k.201229.032.

32 B. Yang, Y. Liu, Q. Liang, M. Chen, L. Ma, L. Li, Q. Liu, W. Tu, D. Lan and Y. Chen, Evaluation of activated carbon synthesized by one-stage and two-stage co-pyrolysis from sludge and coconut shell, *Ecotoxicol. Environ. Saf.*, 2019, **170**, 722–731, DOI: 10.1016/j.ecoenv.2018.11.130.

33 M. A. Hughes, J. A. Allen and S. W. Donne, Characterization of carbonate derived carbons through electrochemical impedance spectroscopy, *Electrochim. Acta*, 2020, **338**, 135847, DOI: 10.1016/j.electacta.2020.135847.

34 H. Wang, Y. Sun, T. Zhu, W. Wang and H. Deng, Adsorption of acetaldehyde onto carbide-derived carbon modified by oxidation, *Chem. Eng. J.*, 2015, **273**, 580–587, DOI: 10.1016/j.cej.2015.03.107.

35 R. Kabir, S. Anwar, S. Yusup, S. Sham, M. Inayat and H. Aminu, Exploring the potential of coconut shell biomass for charcoal production, *Ain Shams Eng. J.*, 2022, **13**(1), 101499, DOI: 10.1016/j.asej.2021.05.013.

36 L. Mishra and G. Basu, Coconut fibre, in *Handbook of Natural Fibres*, Elsevier, 2020, pp. 231–255, DOI: 10.1016/B978-0-12-818398-4.00010-4.

37 C. Saka, BET, TG-DTG, FT-IR, SEM, iodine number analysis and preparation of activated carbon from acorn shell by chemical activation with ZnCl2, *J. Anal. Appl. Pyrolysis*, 2012, **95**, 21–24, DOI: 10.1016/j.jaap.2011.12.020.

38 M. J. Rampe, B. Setiaji and W. Trisunaryanti, Fabrication and characterization of carbon composite from coconut shell carbon, *Indones. J. Chem.*, 2011, **11**(2), 124–130.

39 M. Supeno, R. Siburian and D. Natalia, The Synthesis of Graphene from Coconut Shell Charcoal, in *Proc. 1st Int. Conf. Chem. Sci. Technol. Innov.*, SCITEPRESS, 2019, pp. 39–44, DOI: 10.5220/0008839600390044.

40 U. F. Hassan, A. A. Sallau, O. E. Ekanem, A. Jauro and A. M. Kolo, Effect of carbonization temperature on properties of char from coconut shell, *Int. J. Adv. Chem.*, 2021, **9**(1), 34–39, DOI: 10.14419/ijac.v9i1.31433.

41 K. D. M. S. P. K. Kumarasinghe, G. R. A. Kumara, R. M. G. Rajapakse, D. N. Liyanage and K. Tennakone, Activated coconut shell charcoal based counter electrode for dye-sensitized solar cells, *Org. Electron.*, 2019, **71**, 93–97, DOI: 10.1016/j.orgel.2019.05.009.

42 R. Sari, S. Gea, B. Wirjosentono, S. Hendrana and Y. Hutapea, Improving Quality and Yield Production of Coconut Shell Charcoal Through a Modified Pyrolysis Reactor with Tar Scrubber to Reduce Smoke Pollution, *Pol. J. Environ. Stud.*, 2020, **29**(2), 1815–1824, DOI: 10.15244/pjoes/110582.

43 Y. Li, B. Xing, Y. Ding, X. Han and S. Wang, A critical review of the production and advanced utilization of biochar via selective pyrolysis of lignocellulosic biomass, *Bioresour. Technol.*, 2020, **312**, 123614, DOI: 10.1016/j.biortech.2020.123614.

44 S. Cheng, A. Huang, S. Wang and Q. Zhang, Effect of different heat treatment temperatures on the chemical composition and structure of chinese fir wood, *BioResources*, 2016, **11**(2), 4006–4016, DOI: 10.15376/biores.11.2.4006-4016.

45 A. K. Sakhiya, A. Anand and P. Kaushal, Production, activation, and applications of biochar in recent times, *Biochar*, 2020, 253–285, DOI: 10.1007/s42773-020-00047-1.

46 C. D. Liyanage and M. Pieris, A Physico-Chemical Analysis of Coconut Shell Powder, *Procedia Chem.*, 2015, **16**, 222–228, DOI: 10.1016/j.proche.2015.12.045.

47 O. Oginni, K. Singh, G. Oporto, B. Dawson-Andoh, L. McDonald and E. Sabolsky, Influence of one-step and two- step KOH activation on activated carbon characteristics, *Bioresour. Technol. Rep.*, 2019, **7**, 100266, DOI: 10.1016/j.biteb.2019.100266.

48 D. Castilla-Caballero, J. Barraza-Burgos, S. Gunasekaran, A. Roa-Espinosa, J. Colina-Márquez, F. Machuca-Martínez, A. Hernández-Ramírez and S. Vázquez-Rodríguez, Experimental data on the production and characterization of biochars derived from coconut-shell wastes obtained from the Colombian Pacific Coast at low temperature pyrolysis, *Data Brief*, 2020, **28**, 104855, DOI: 10.1016/j.dib.2019.104855.

49 L. Muniandy, F. Adam, A. R. Mohamed and E. P. Ng, The synthesis and characterization of high purity mixed microporous/mesoporous activated carbon from rice husk using chemical activation with NaOH and KOH, *Microporous Mesoporous Mater.*, 2014, **197**, 316–323, DOI: 10.1016/j.micromeso.2014.06.020.

50 A. Nyamful, E. K. Nyogbe, L. Mohammed, M. N. Zainudeen, S. A. Darkwa, I. Phiri, M. Mohammed and J. M. Ko, Processing and Characterization of Activated Carbon from Coconut Shell and Palm Kernel Shell Waste by H_3PO_4 Activation, *Ghana J. Sci.*, 2021, **61**(2), 91–104, DOI: 10.4314/gjs.v61i2.9.

51 M. S. Islam, B. C. Ang, S. Gharehkhani and A. B. M. Afifi, Adsorption capability of activated carbon synthesized from coconut shell, *Carbon Lett.*, 2016, **20**, 1–9, DOI: 10.5714/CL.2016.20.001.

52 B. Kwasi Opoku, A. Isaac, A. Akrofi Micheal, J. Kwesi Bentum and W. Paul Muyoma, Characterization of Chemically Activated Carbons Produced from Coconut and Palm Kernel Shells Using SEM and FTIR Analyses, *Am. J. Appl. Chem.*, 2021, **9**(3), 90, DOI: 10.11648/j.ajac.20210903.15.

53 A. Valencia, R. Muñiz-Valencia, S. G. Ceballos-Magaña, C. K. Rojas-Mayorga, A. Bonilla-Petriciolet, J. González and I. A. Aguayo-Villarreal, Cyclohexane and benzene separation by fixed-bed adsorption on activated carbons prepared from coconut shell, *Environ. Technol. Innov.*, 2022, **25**, 102076, DOI: 10.1016/j.eti.2021.102076.

54 Y. Gao, Q. Yue, B. Gao and A. Li, Science of the Total Environment Insight into activated carbon from different kinds of chemical activating agents : A review, *Sci. Total Environ.*, 2020, **746**, 141094, DOI: 10.1016/j.scitotenv.2020.141094.

55 L. Zhang, L. Y. Tu, Y. Liang, Q. Chen, Z. S. Li, C. H. Li, Z. H. Wang and W. Li, Coconut-based activated carbon fibers for efficient adsorption of various organic dyes, *RSC Adv.*, 2018, **8**(74), 42280–42291, DOI: 10.1039/c8ra08990f.

56 Y. Chen, L. J. Zhou, Y. Z. Hong, F. Cao, L. Li and J. B. Li, Preparation of high-surface-area activated carbon from coconut shell fibers, *Xinxing Tan Cailiao/New Carbon Mater.*, 2010, **25**(2), 151–155, DOI: 10.1016/j.carbon.2010.03.059.

57 T. S. Hui and M. A. A. Zaini, Potassium hydroxide activation of activated carbon: A commentary, *Carbon Lett.*, 2015, **16**(4), 275–280, DOI: 10.5714/CL.2015.16.4.275.

58 B. Sajjadi, T. Zubatiuk, D. Leszczynska, J. Leszczynski and W. Y. Chen, Chemical activation of biochar for energy and environmental applications: a comprehensive review, *Rev. Chem. Eng.*, 2019, **35**(7), 777–815, DOI: 10.1515/revce-2018-0003.

59 C. Song, S. Wu, M. Cheng, P. Tao, M. Shao and G. Gao, Adsorption studies of coconut shell carbons prepared by KOH activation for removal of lead(ii) from aqueous solutions, *Sustainability*, 2014, **6**(1), 86–98, DOI: 10.3390/su6010086.

60 W. Widiyastuti, M. Fahrudin Rois, N. M. I. P. Suari and H. Setyawan, Activated carbon nanofibers derived from coconut shell charcoal for dye removal application, *Adv. Powder Technol.*, 2020, **31**(8), 3267–3273, DOI: 10.1016/j.apt.2020.06.012.

61 R. Liu, J. X. Wang and W. D. Yang, Hierarchical Porous Heteroatoms—Co-Doped Activated Carbon Synthesized from Coconut Shell and Its Application for Supercapacitors, *Nanomaterials*, 2022, **12**(19), 3504, DOI: 10.3390/nano12193504.

62 E. Budi, Umiatin, H. Nasbey, R. A. Bintoro, F. Wulandari and Erlina, Activated coconut shell charcoal carbon using chemical-physical activation, *AIP Conf. Proc.*, 2016, **1712**, 040081, DOI: 10.1063/1.4941886.

63 M. Ataeefard, A. Shadman, M. R. Saeb and Y. Mohammadi, A hybrid mathematical model for controlling particle size, particle size distribution, and color properties of toner particles, *Appl. Phys. A: Mater. Sci. Process.*, 2016, **122**(8), 1–14, DOI: 10.1007/s00339-016-0242-1.

64 T. Bhongade, Gogaram, D. M. Gautam and R. P. Vijayakumar, Synthesis of MWCNTs using waste toner powder as carbon source by chemical vapor deposition method, *Fullerenes, Nanotub. Carbon Nanostruct.*, 2019, **27**(11), 864–872, DOI: 10.1080/1536383X.2019.1652169.

65 J. Yang, T. J. Wang, H. He, F. Wei and Y. Jin, Particle Size Distribution and Morphology of in Situ Suspension Polymerized Toner, *Ind. Eng. Chem. Res.*, 2003, **42**(22), 5568–5575, DOI: 10.1021/ie0301029.

66 Z. Bazrafshan, M. Ataeefard and F. Nourmohammadian, Physicochemical colourants effects on polymeric composites printing toner, *Pigment Resin Technol.*, 2014, **43**(5), 245–250, DOI: 10.1108/PRT-09-2013-0085.

67 S. M. Omokafe, A. A. Adeniyi, E. O. Igbafen, S. R. Oke and P. A. Olubambi, Fabrication of Activated Carbon from Coconut Shells and its Electrochemical Properties for Supercapacitors, *Int. J. Electrochem. Sci.*, 2020, **15**(11), 10854–10865, DOI: 10.20964/2020.11.10.

68 I. Ismail, Arliyani, S. Fathmiyah, Mursal, Z. Jalil and H. P. S. A. Khalil, Effect of ball-milling time on chemical property of coconut shell powder, *J. Phys., Conf. Ser.*, 2020, **1572**(1), 012021, DOI: 10.1088/1742-6596/1572/1/012021.

69 R. S. S. Raju and G. S. Rao, Assessment of tribological performance of coconut shell ash particle reinforced Al-Si-Fe composites using grey-fuzzy approach, *Tribol. Int.*, 2017, **39**(3), 364–377, DOI: 10.24874/ti.2017.39.03.12.

70 A. I. Bakti and P. L. Gareso, Characterization of Active Carbon Prepared from Coconuts Shells using FTIR, XRD and SEM Techniques, *J. Ilm. Pendidik. Fis. Al-Biruni*, 2018, **7**(1), 33–39, DOI: 10.24042/jipfalbiruni.v7i1.2459.

71 M. Olán Ramos, E. Del Angel Meraz, J. M. Rojo, D. E. Pacheco-Catalán, M. A. Pantoja Castro and R. S. Mora Ortiz, Activated carbons from coconut shell and NiO-based composites for energy storage systems, *J. Mater. Sci. Mater. Electron.*, 2021, **32**(4), 4872–4884, DOI: 10.1007/s10854-020-05227-0.

72 N. Othman, M. H. Hussin, R. K. Shuib and N. Sulaiman, Comparison characteristic between milled coconut shell activated carbon powder and carbon black: Physical, chemical and morphological properties, *AIP Conf. Proc.*, 2018, **1985**, 040003, DOI: 10.1063/1.5047187.

73 M. D. Obradović, G. D. Vuković, S. I. Stevanović, V. V. Panić, P. S. Uskoković, A. Kowal and S. L. Gojković, A comparative study of the electrochemical properties of carbon nanotubes and carbon black, *J. Electroanal. Chem.*, 2009, **634**(1), 22–30, DOI: 10.1016/j.jelechem.2009.07.001.

74 T. C. de Oliveira Cândido, A. C. Pereira and D. N. da Silva, Development and Characterization of Conductive Ink Composed of Graphite and Carbon Black for Application in Printed Electrodes, *Analytica*, 2023, **4**(4), 513–526, DOI: 10.3390/analytica4040035.

75 M. Rosi, M. N. Z. Fatmizal, D. H. Siburian and A. Ismardi, Activated Carbon Prepared From Coconut Shell Powder With Low Activation Time As Supercapacitor Electrodes, *Indones. Phys. Rev.*, 2023, **6**(1), 85–94, DOI: 10.29303/ipr.v6i1.205.

76 C. Schütter, C. Ramirez-Castro, M. Oljaca, S. Passerini, M. Winter and A. Balducci, Activated Carbon, Carbon Blacks and Graphene Based Nanoplatelets as Active Materials for Electrochemical Double Layer Capacitors: A Comparative Study, *J. Electrochem. Soc.*, 2015, **162**(1), A44–A51, DOI: 10.1149/2.0381501jes.

77 J. H. Anderson, Effects of Carbon Black on Toner Tribocharging in Two-Component Electrophotographic Developers, *J. Imaging Sci. Technol.*, 2001, **45**, 529–536, DOI: 10.2352/J.ImagingSci.Technol.2001.45.6.art00005.

78 P. U. Okoye, C. Alegre and D. Ram, A review on carbon materials for electrochemical energy storage applications: State of the art, implementation, and synergy with metallic compounds for supercapacitor and battery electrodes, *J. Power Sources*, 2024, **617**, 235140, DOI: 10.1016/j.jpowsour.2024.235140.

79 G. Inzelt and G. G. Láng, Electrochemical Impedance Spectroscopy (EIS) for Polymer Characterization, in *Electropolymerization*, ed. S. Cosnier and A. Karyakin, Wiley-VCH, Weinheim, Germany, 2010, pp. 51–76.

80 A. Motaghi, A. N. Hrymak and G. H. Motlagh, Electrical conductivity and percolation threshold of hybrid carbon/polymer composites, *J. Appl. Polym. Sci.*, 2015, **132**, 41744, DOI: 10.1002/app.41744.

81 A. L. Cazetta, O. P. Junior, A. M. M. Vargas, A. P. Da Silva, X. Zou, T. Asefa and V. C. Almeida, Thermal regeneration study of high surface area activated carbon obtained from coconut shell: Characterization and application of response surface methodology, *J. Anal. Appl. Pyrolysis*, 2013, **101**, 53–60, DOI: 10.1016/j.jaap.2013.02.013.

82 B. Strzemiecka, A. Voelkel, J. Donate-Robles and J. M. Martín-Martínez, Assessment of the surface chemistry of carbon blacks by TGA-MS, XPS and inverse gas chromatography using statistical chemometric analysis, *Appl. Surf. Sci.*, 2014, **316**(1), 315–323, DOI: 10.1016/j.apsusc.2014.07.174.

83 S. J. Potts, T. Korochkina, A. Holder, E. Jewell, C. Phillips and T. Claypole, The influence of carbon morphologies and concentrations on the rheology and electrical performance of screen-printed carbon pastes, *J. Mater. Sci.*, 2022, **57**(4), 2650–2666, DOI: 10.1007/s10853-021-06724-1.

84 M. Ali, L. Li and D. Cartridge, Progress in Organic Coatings High electrical conductivity waterborne dispersions of carbon black pigment, *Prog. Org. Coating*, 2019, **129**, 199–208, DOI: 10.1016/j.porgcoat.2018.12.010.